The Automatic Recognition of Large Ball Valve Sealing Bolt Based on Digital Image

Qingjun Song[1], Xingming Xiao[2] and Haiyan Jiang[3]

[1,2]*School of Mechanical and Electrical Engineering, China University of Mining & Technology, Xuzhou*
[3]*School of Tai-An, Shandong University of Science & Technology, Tai-an*
*qjsong76@126.com[1], xl6265@cumt.edu.cn[2], littlsunny@163.com[3]*

Abstract

In this paper, we put forward an effective algorithm for edge detection based on combination of multi-shape/scale Mathematical morphology and wavelet transformation. Firstly, the bimodal method and multi-threshold method were combined for the image segmentation. Then, the image edge was detected by the algorithm. Finally, the angle between the bolt and manipulator was calculated using the rotation conversion matrix. With the systematic error and correlation coefficient, the calculated angle was verified. Experimental results show that the method can protect the edge integrity of the nut image, with fast processing speed and strong anti-noise ability. The work in this paper provides a theoretical basis for the automatic recognition in the large ball valve sealing bolt system.

Keywords: *Mathematical morphology, Wavelet transformation, Edge detection, Angle recognition, Systematic error, Correlation coefficient*

1. Introduction

In the turbine inlet system, the large ball valves are installed in a high altitude with manual operation for the gap adjustment in process. The very narrow space accretes the labor intensity of workers. Therefore, the gap adjusting time is longer. Moreover, it is very inconvenient in production with manual operation. In order to improve the working conditions, we developed a large ball valve sealing bolt auto-adjusting system. The system is mainly composed of the orbit determination device, traveling mechanism, manipulator, sensors and the control unit. The three-dimensional computer assemble model is shown in Figure 1. The field installation is shown in Figure 2, Figure 2 (a) is the initial state of the manipulator, Figure 2 (b) is its working state.
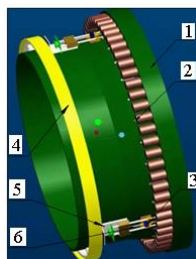
**Figure 1.Three-dimension Model of the Auto-adjusting System**

(1) Ball valve shell; (2) Sealing bolt ;(3) Sensor; (4) Orbit determination device; (5) Traveling mechanism; (6) Manipulator

(a) Initial state of manipulator   (b) Working state of manipulator
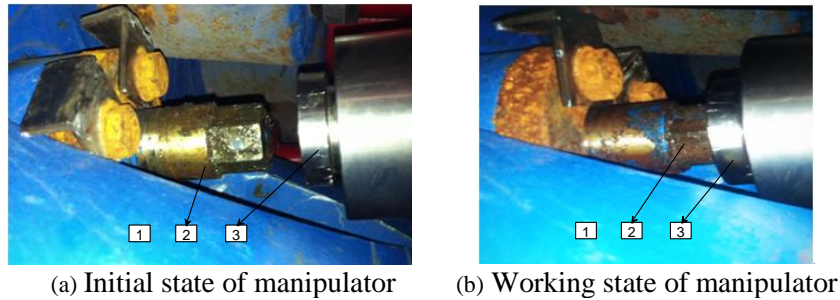
Figure 2. Field Installation Picture

(1) Ball valve shell; (2) Sealing bolt; (3) Manipulator

The orbit determination device is installed on the outer of the large ball valve, which is positioned by a large internal gear drive. The sensors are used for sending the position information of the sealing bolt to the controller. The ball valve sealing gap is adjusted automatically by three manipulators uniformly distributed in the orbit determination device. However, there is a problem that the hexagons of the bolt nut and manipulator usually mismatch (see Figure 3). Therefore, how to recognize the angle θ between the bolt and manipulator is critical for the auto-adjusting system.
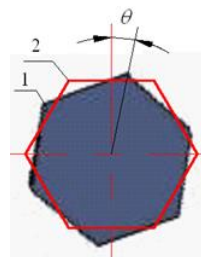
Figure 3.Sketch of the Installation Position

1. Position of the bolt; 2. Initial position of the manipulator

There are many traditional edge detection methods, such as Sobel operator, Robert operator, Prewitt operator, Log operator and Canny, based on calculating the difference in a small local area of the image. Zhou *et al.* and He *et al.* [1, 2] proved that these operators are more sensitive to noise; furthermore the noise will be strengthened in the edge detection. Mathematical morphology has been widely used for image analysis and recognition [3].And the mathematical morphology edge detection operator mainly using morphological gradient does not strengthen the noise, although it is also sensitive to the noise. As mentioned in [4, 5], mathematical morphology is a nonlinear filtering method, in which the structure elements with certain forms is used to measure and extract the image edge for analysis and target recognition.

Mathematical morphology algorithm has good edge detection ability, but its noise-resisting ability is relatively low [6]. Wavelet transforms have great superiority in image denoising. So we give an edge detection method based on combination of multi-shape/scale Mathematical morphology and wavelet transformation. In addition, a way of recognizing the angle θ between the bolt and manipulator is presented with geometrical feature extraction and graph conversion matrix, achieving accurate positioning manipulators.

2. Image Processing

2.1 Image Preprocessing

In order to eliminate the useless information, the color image is converted to gray image through the weighted average method [7, 8]. Additionally, the holes in the nut characters are filled to maintain the integrity of the information.

During the binary conversion, since the peak valley of the nut image histogram is unobvious, not obvious, Sonka *et al.* [9] proposed that it is difficult to obtain satisfactory results only using the single-threshold image segmentation method. Thus, the bimodal method and multi-threshold method are combined for the image segmentation. Suppose that $G(x, y)$ is the grey image, $Z(i, j)$ is the gray value of the point (i, j), Z_{max} is the peak valley of the histogram, which is defined as the grey threshold of image segmentation, Z_{min} is the smallest gray threshold, then $Z(i, j)$ can be expressed as

$$Z(i, j) = \begin{cases} 0 & Z(i, j) \leq Z_{min} \\ \dfrac{255[Z(i, j) - Z_{min}]}{Z_{max} - Z_{min}} & Z_{min} < Z(i, j) < Z_{max} \\ 255 & Z(i, j) \geq Z_{max} \end{cases} \tag{1}$$

The six edge points of the multi-threshold preliminary processing image are assumed to be the seed, *i.e.*, and the growth starting point in the background region [10]. If the adjacent gray difference (4-connected) is less than a given threshold, the pixels are thought of belonging to the same image region and are merged into one region. Otherwise, they belong to different image regions. Set S is the seed point (x_0, y_0) in the *(k-1)*-th filled region, the coordinates collection F_K in the *k*-th filling can be defined as

$$F_K = F_{K-1} \bigcup \{(x_0 + 1, y_0), (x_0 - 1, y_0), (x_0, y_0 + 1), (x_0, y_0 - 1)\} \quad C(i, j) = 1 \tag{2}$$

where $C(i, j)$ is the gray filled condition, and F_{K-1} is the coordinates collection in the *(k-1)*-th filling.

If the gray value of S is $Z(x_0, y_0)$, and the adjacent gray value to the seed S is $Z(x_0^{'}, y_0^{'})$, the gray conformity formula can be expressed as follows

$$\gamma = \frac{|Z(x_0, y_0) - Z(x_0', y_0')|}{Z(x_0, y_0)} \times 100\% \tag{3}$$

So that,

$$C(i, j) = \begin{cases} 1, & if \quad 0 \leq \gamma < M \\ 0, & if \quad M \leq \gamma \leq 100\% \end{cases} \tag{4}$$

where M is a constant value of grey conformity.

The preprocessing images are shown in Figure 4.

(a) Gray image; (b) Image of area filling; (c) binary image

Figure 4. Preprocessing Images

2.2 Image Edge Detection based on Wavelet Transformation

Wavelet transforms have been widely used for image denoising since they provide a suitable basis for separating noisy [11]. Suppose that the preprocessed image *G(x,y)* of

size $m \times n$ has been decomposed through a discrete wavelet transform. We can obtain four subbands, denoted by low-low (LL), low-high (LH), high-low (HL), and high-high (HH). The low subbands correspond to details of the image, and the HH subband can contain a significant amount of noise, so the effect of image denoising can be achieved through adjusting wavelet decomposition coefficient threshold.

The noise standard deviation denoted by σ_n, is given by [11]

$$\sigma_n = \frac{median(|W_{i,j}|)}{0.6745} \qquad |W_{i,j}| \in subband \;\; \mathrm{HH} \tag{5}$$

Here we use another standard deviation to estimate the original image, denoted by σ_x, that is got by

$$\sigma_x = \sqrt{\left| \sigma_y^2 - \sigma_n^2 \right|} \tag{6}$$

where $\sigma_y^2 = \frac{1}{N_S} \sum_{i,j=1}^{N_S} W_{i,j}^2$, N_S is the number of wavelet coefficients $W_{i,j}$ on the high subband.

Then the adaptive threshold is given by T_m

$$T_m = \lambda_m \frac{\sigma_n}{\sigma_x} \tag{7}$$

where $\lambda_m = \sqrt{m \log(N_m / M)}$ is adaptive factor at m-th decomposition level, and $m = 1,...,M$, M is the total decomposition level, N_m represents coefficients size at m-th decomposition level.

The wavelet transforms based on adaptive threshold method is used to effectively reduce noise while preserving important features of the original image.

The basic thought Mathematical Morphology is to measure and detect an image shapes in order to analyze and recognize image by using structure element .Tang et al. and Sun *et al.* [12, 13] after analyzing different element, pointed out the multi-structure elements and multi-scale elements edge detection algorithm which was used to find the details of object, while, the algorithm was not expressed in an exact number and used in the engineering. By comparing the test result and the operation time among structural elements with the scale of 3, 5, and 7, the scale of structural elements is designed as 5 and 3. The structure elements are shown in Figure 5, whereas the black box demonstrates the origin of structural elements.
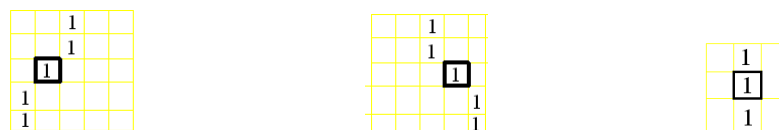
a) 60° structure elements; b) 120° structure elements; c) 90° structure elements

Figure 5. Structure Elements

Ref. [7, 8] demonstrated the two basic arithmetic operations, *i.e.*, erosion and dilation, in the mathematical morphology. The erosion and dilation are not inverse but concatenated operation in edge detection [14]. In order to make full use of the advantages of different structural elements, the morphology edge detection algorithm was proposed based on the multi-shape/scale structural elements. With the definition that $\phi(G)$ denotes the boundary of the input image G, and $B_i (0 < i \le n)$ represents a group of structural elements, the edge detection operator is written as

$$\phi(G) = \frac{1}{n} \sum_{i=1}^{n} [((G \oplus B_i) - (G \ominus B_i)) \ominus B_i] \tag{8}$$

where n indicates the scale, and $n=3$ is chosen. The structural elements of B_i are given in Fig. 5. $G \oplus B$ indicates that G is dilated by B, and $G \oplus B = \{x \mid [(\hat{B})_x \bigcap G] \neq \Phi\}$. $G \Theta B$ indicates that G is eroded by B, and $G \Theta B = \{x \mid (B)_x \subseteq G\}$.

Fig. 6 is the result of the nut image edge detection, and it shows that the proposed algorithm can accurately detect the details of the edges, making the image outlines clear, complete and coherent.
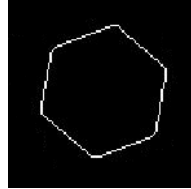

Figure 6. Result of the Edge Detection

3. Recognition of the Shape Feature Points of Nut

3.1 Conversion of the Coordinate

The coordinate origin of the image is usually set at (0, 0). However, in our recognizing work the coordinate system must be conversed to the middle of the image as the origin. Suppose that P_0 and P denote the coordinate matrices before and after the conversion, respectively. The coordinate conversion model is as follows

$$P = TP_0 \tag{9}$$

where T is the conversion coordinate matrix, so the new coordinate is got by

$$P = TP_0 = \begin{pmatrix} 1 & 0 & N/2 \\ 0 & 1 & M/2 \\ 0 & 0 & 1 \end{pmatrix} \cdot \begin{pmatrix} 0 \\ 0 \\ 1 \end{pmatrix} = \begin{pmatrix} N/2 \\ M/2 \\ 1 \end{pmatrix} \tag{10}$$

3.2 Extraction of the Shape Feature points

For the $m \times n$ object image, the centre of the shape can be obtained with the following expression below.

$$\begin{cases} \overline{x} = \dfrac{1}{mn} \sum_{i=0}^{n-1} \sum_{j=0}^{m-1} x_i \\ \overline{y} = \dfrac{1}{mn} \sum_{i=0}^{n-1} \sum_{j=0}^{m-1} y_i \end{cases} \tag{11}$$

The feature shape points of the nut are defined as A, B, C, D, E and F. The distance DI from the edge point to the centre can be expressed as

$$DI(O,M) = \sqrt{(\overline{x} - x_M)^2 + (\overline{y} - y_M)^2} \tag{12}$$

where O is the centre point $(\overline{x}, \overline{y})$ of the nut, M is the point (x_M, y_M) on the edge of the shape.

According to the characteristics of the hexagon, the distances (AO, BO, CO, DO, EO and FO)
are the greatest and equal. The set of the greatest distances is defined as the feature point matrix
DI_{max} with the following form as

$$DI_{max} = \max[\sqrt{(\bar{x} - x_M)^2 + (\bar{y} - y_M)^2}]$$

$$= \begin{pmatrix} x_A & y_A \\ x_B & y_B \\ x_C & y_C \\ x_D & y_D \\ x_E & y_E \\ x_F & y_F \end{pmatrix} \qquad (13)$$

where the feature point A must be in the first quadrant, i.e., both x_A and y_A are positive.

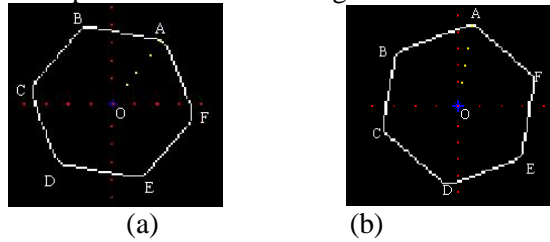The center and shape feature points are shown in Figure 7.

(a)　　　　　(b)

Figure 7. Illustration of the Feature Points

A thorough study of the images about bolt at different positions was carried out. It is found that two cases decide the direction and angle of manipulator rotation. One case is that there is only one feature point (A) in the first quadrant (Figure 7(a)), the other is that there are two feature points (A and F) in the first quadrant (Figure 7 (b)).

4. Recognition of Angle between Manipulator and Bolt

The initial position of the manipulator is fixed (Figure 3 (1)), while the position of the bolt (Figure 3(2)) is random. The manipulator needs to rotate an angle θ to fit the nut of the bolt. DI_{max}' is defined as the feature point matrix $DI_{max}' = [A'\ B'\ C'\ D'\ E'\ F']$ after rotating, θ is the rotating angle, the rotating formula is expressed as

$$DI_{max} \cdot F = DI_{max}' \qquad (14)$$

where F is the rotation conversion matrix, $F = \begin{pmatrix} \cos\theta & \sin\theta \\ -\sin\theta & \cos\theta \end{pmatrix}$.

Eq.(14) can be rearranged as

$$\begin{pmatrix} x_A & y_A \\ x_B & y_B \\ x_C & y_C \\ x_D & y_D \\ x_E & y_E \\ x_F & y_F \end{pmatrix} \cdot \begin{pmatrix} \cos\theta & \sin\theta \\ -\sin\theta & \cos\theta \end{pmatrix} = \begin{pmatrix} x_A' & y_A' \\ x_B' & y_B' \\ x_C' & y_C' \\ x_D' & y_D' \\ x_E' & y_E' \\ x_F' & y_F' \end{pmatrix} \qquad (15)$$

Since the feature point in the first quadrant determines the angle and direction of rotation, point A is chosen to calculate the rotation angle. Eq. (16) can be deduced to

$$\begin{cases} x_A \cos\theta - y_A \sin\theta = x_A' \\ x_A \sin\theta + y_A \cos\theta = y_A' \end{cases} \qquad (16)$$

According to Eq. (16), we obtain the rotation angle as follows:

$$\theta = \arccos(\frac{x_A \cdot x_A{}' + y_A y_A{}'}{x_A{}^2 + y_A{}^2}) \tag{17}$$

If there is only one feature point in the first quadrant as Fig. 7(a), the manipulator rotates $(60-\theta)°$ in the counterclockwise direction. If there are two feature points in the first quadrant and the abscissa value of the feature point A is the biggest as Fig. 7(b), the manipulator rotates $\theta°$ in the clockwise direction.

5. Discussion

To judge the accuracy of rotational angle, a measurement in mathematics must be established. $G_{m\times n}$ denotes the gray matrix of image profile after rotation with the grey value $g(i,j)$, and $H_{m\times n}$ is the gray matrix of standard image profile with the grey value $h(i,j)$. The accuracy of recognition is normalized as the correlation coefficient R [15, 16].

$$R = \frac{cov(G,H)}{\sqrt{D(G)} \bullet \sqrt{D(H)}} = \frac{\sum_{i=1}^{m}\sum_{j=1}^{n}[g(i,j)-\bar{g}] \bullet [h(i,j)-\bar{h}]}{\sqrt{\sum_{i=1}^{m}\sum_{j=1}^{n}[g(i,j)-\bar{g}]^2} \bullet \sqrt{\sum_{i=1}^{m}\sum_{j=1}^{n}[h(i,j)-\bar{h}]^2}} \tag{18}$$

where $cov(G,H)$ is the gray covariance of rotating and standard images, $\sqrt{D(G)}$ and $\sqrt{D(H)}$ are the standard deviation, $\bar{g}$ and $\bar{h}$ are the gray average. The greater $R \in [0,1]$ is, the more accurate the rotational angle is. When $R = 1$, the rotational angle is completely accurate.

It has been generally accepted that the measuring accuracy of digital image processing can achieve 0.01 pixels [17]. However, Ref. [18, 19] indicated there are systematic errors due to sub-pixel reconstruction, illumination intensity changes, thermal noise, environmental factors, and other factors. In order to improve the recognition robustness for reducing the systematic error, we analyzed Eq.(18) and derived the new expressions of correlation coefficient as follows.

$$R = \frac{\sum_{k=1}^{m/10}\sum_{i=1}^{m}\sum_{j=1}^{n}\omega_k\{[g(i,j)-\bar{f}] \bullet [h(i,j)-\bar{h}]\}}{\sqrt{\sum_{i=1}^{m}\sum_{j=1}^{n}[g(i,j)-\bar{g}]^2} \bullet \sqrt{\sum_{i=1}^{m}\sum_{j=1}^{n}[h(i,j)-\bar{h}]^2}} \tag{19}$$

where ω_k is the weighting coefficient, $\omega_k = \sum_{k=0}^{l}\frac{10}{m|\delta_k - \delta_0|}$. δ_0 and δ_k are the grey average and grey value of image edge pixels, respectively. l is the maximum gray. If $|\delta_k - \delta_0| = 0$, $\omega_k = 1$; if $|\delta_k - \delta_0| = 1$, $\omega_k = 0$.

In order to quantitatively analyze the accuracy of rotational angle and to improve the measurement precision, the systematic error is defined as

$$\gamma = \sqrt{\frac{\sum_{i=1}^{m}\sum_{j=1}^{n}[f(i,j)-g(i,j)]^2}{m \times n}} \times 100\% \tag{20}$$

where, the closer to zero $\gamma \in [0,1]$ is, the higher the accuracy is.

The bolts with several different angles were identified and tested using the image processing methods above. The systematic error and the rotation error of every edge pixel are calculated according to Eq. (20). The image used was 128×128 pixel in size, where

$60 \times 60 = 3600$ pixel points were calculated. As seen from Figure (8), the large error mainly concentrates in the middle part of the image due to the bolt craft hole. The error in the edge is very small, proving that the algorithm is efficient on the recognition of edges and can meet the requirement of the bolt rotation measurement.
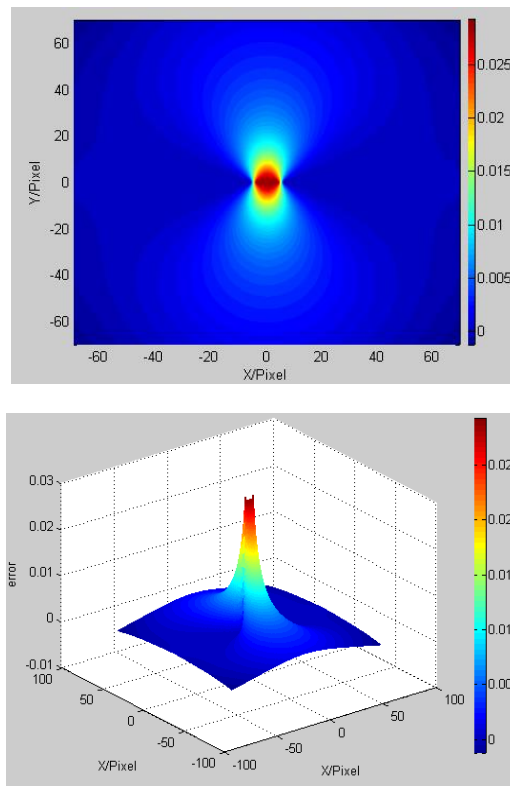
(a) Scatter pseudo color map of error   (b) 3D surface of error

Figure 8. Analysis Diagram of Measurement Error

In addition, the correlation coefficient was calculated, shown in Table 1.

Table 1. Results Analysis Information

Index	$\theta = 3°$ (*clockwise*)	$\theta = 4°$ (*clockwise*)	$\theta = 3°$ (*counterclockwise*)	$\theta = 4°$ (*counterclockwise*)
R	0.990	0.993	0.991	0.992
γ	0.017	0.019	0.018	0.019

For both clockwise and counterclockwise rotations, the correlation coefficient R is very close to 1. The computing time is 29s with the systematic error $\gamma < 0.02$. This proves that the algorithm can accurately identify the characteristic parameters of the sealed bolt, and then the manipulator can be exactly positioned.

6. Conclusions

In image recognition, for a single image edge detection is easily affected by noise, which leads to the problem of poor effect of edge extraction. In this paper, we propose a new edge detection algorithm based on wavelet transform and mathematical morphology. Additionally, we give an image measurement method for engineering application. The expression of the image gray correlation with weighted coefficient is put forward in this

paper. Moreover, the systematic error was derived from the classical measurement error. The system not only has good robustness, but also ensures the processing speed with certain feasibility. Random bolt positions were created with variable angles to examine different situations. The experimental results in Tai-shan pumped-storage power station show that the algorithm has good denoising ability and edge connectivity for the blurred but not too complex images. The system can accurately recognize the position of the bolt. With the Scatter map and 3D surface of error, the accuracy of bolt rotation was verified, proving that the automatic recognition of large ball valve sealing bolt can be well achieved.

Acknowledgments

References

[1]   J. X. Zhou and G. P. Wu, "A Combined edge detecting based on median filter and mathematics morphology," Modern Computer, vol. 2, (2005), pp. 73-75.
[2]   K. X. He and Q. Wang, "Image edge detection based on nonsubsampled contourlet transform and mathematical morphology," Journal of Southeast University (English Edition), vol. 28, (2012), pp. 445 - 449.
[3]   Xi. Zh. B, F. G. Zhou and B. D. Xue, "Discrimination ability improvement of invariant moment based on multi-scale mathematical morphology", Optik., vol. 124, (2013), pp.1314-1319.
[4]   P. B. Ramkumar and K. V. Pramod, "Convex geometry and mathematical morphology in a generalized structure," International Journal of Computer Applications, vol. 6, (2010), pp. 1-6.
[5]   J. L. Huang and H. Zou, "An image edge detection method of multi-structure elements and multi- scale based on morphology," Microelectronics & Computer, vol. 26, (2009), pp. 149-153.
[6]   H. Lin, P. J. Du, Ch. Sh. Zhao, N. Shu , "Edge detection method of remote of remote sensing images based on mathematical morphology of multi-structure elements," Chinese geographical science, vol. 14, no. 3, (2004), pp. 63-268.
[7]   R. C. Gonzalez and R. E. Woods, "Digital Image Processing Using MATLAB," Publishing House of Electronics Industry, Beijing (2012).
[8]   W. K. Pratt, "Digital Image Processing," Academic Press, New York (1991).
[9]   M. Sonka, V. Hlavac and R. Boyle, "Image processing, analysis, and machine vision," Thomson Asia Pte Led, (2002).
[10] X. Li, G. Wei, X. D. Bian, "Research on detection of lane based on machine vision," Journal of Southeast University (English Edition), (2004), pp.176 -179.
[11] R. D. Silva, R. Minetto ,W. R. Schwartz and H. Pedrini, "Adaptive edge-preserving image denoising using wavelet transforms, "Pattern Anal Applic., vol. 16, (2013), pp. 567-580.
[12] Y. H. Tang and H. Zh. Lu, "Morphological edge detection algorithm based on multi-structure elements compound filter," Geomantics and Information Science of Wuhan University, vol. 37, (2012), pp. 50-53.
[13] J. X. Sun and D. B. Gu, "A multi-scale edge detection algorithm based on wavelet domain vector hidden Markova tree model," Pattern Recognition, vol. 7, (2004), pp. 1315-1324.
[14] Y. T. Zhang, Z. K.Yin and J. Y. Wang, "A new image edge detection scheme," Journal of Electronics & Information Technology, vol. 30, (2008), pp. 1295-1299.
[15] W. J. Maclean and J. K. Tsotsos, "Fast pattern recognition using normalized grey-scale correlation in a pyramid image representation," Machine Vision and Applications, vol. 19, (2008), pp. 163-179.
[16] J. Y. Yan. and J. G. Yang, "Application of synthetic grey correlation theory on thermal point optimization for machine tool thermal error compensation," Int J Adv Manuf Technol, vol. 43, (2009), pp. 1124-1132.
[17] H. W. Wang, Y. L. Kang and H. P. Xie, "Advance in digital speckle correlation method and its application," Advances in Mechanics, vol. 35, (2005), pp. 195-203.
[18] H. W. Schreier and A. Michael, "Systematic error in digital image correlation due to under matched subset shapes," Experimental Mechanics, vol. 42, (2002), pp. 303-310.
[19] H. W. Schreier and M. A. Sotton, "Systematic errors in digital image correlation caused by intensity interpolation," Opt Eng, vol. 36, (2002), pp. 2361-2361.